Possible link between guanosine 5′ triphosphate hydrolysis and solitary waves in microtubules

B. Trpišová and J. A. Tuszyński
Department of Physics, University of Alberta, Edmonton, Alberta, Canada T6G 2J1
(Received 10 September 1996)

The cytoskeleton of eucaryotic cells is composed of several classes of protein polymers among which microtubules (MTs) are the most prominent. Microtubules are important in a variety of cellular activities but the physical reasons underlying their behavior are largely unknown. Inside the cell they usually exist in an unstable dynamic state characterized by a continuous addition and dissociation of the molecules of tubulin. The addition of each tubulin is accompanied by the hydrolysis of guanosine 5′ triphosphate bound to the β monomer of the molecule. Experiments show that an amount of energy comparable to 6.25×10^{-21} J is freed in this reaction. A few researchers have put forward a hypothesis that this energy can travel along MTs as a kinklike solitary wave. In this paper two models are analyzed whose special solutions are traveling kinks that arise as a result of coupling between dielectric and elastic degrees of freedom of tubulin. By means of these models a collision of the kink wave with an impurity in the microtubule is studied. The impurity may represent a protein attached to the microtubule or a structural discontinuity in the arrangement of the tubulin molecules. We conjecture that the collisions of the quanta of energy propagating in the form of kinks with such defects may explain some features of the microtubule behavior. [S1063-651X(97)12503-X]

PACS number(s): 87.15.He, 62.30.+d, 63.20.Mt, 64.60.Cn

I. INTRODUCTION

Microtubules (MTs) are cylindrical protein structures that are the major constituent part of the cytoskeleton of all eucaryotic cells. They have a form of hollow tubes whose walls are assembled from the molecules of globular protein tubulin. Tubulin is an approximately 8×10^{-9}-m-long dimer composed of two monomers, α- and β-tubulin, each with a molecular weight 50–55 kilodaltons. Molecules of tubulin in MTs form parallel protofilaments that are longitudinally shifted with respect to each other, which results in a helical arrangement of the tubulin subunits in the MT wall (Fig. 1). Most observed MTs have 13 or 14 protofilaments [1]. This corresponds to a MT diameter of approximately 25×10^{-9} m. The length of an intermediate MT is about 10^{-6} m. In the axons of neurons they can be as long as several centimeters.

MTs participate in various cellular events. During cell division they extend from two centrosomes located at the opposite poles of the dividing cell and attach to the sister chromatids of each chromosome [2]. In anaphase the chromatids are pulled apart by shortening MTs so that an equal number of chromosomes is assigned to each of the two future daughter cells. In nondividing cells MTs form an array around the centrosome that is positioned close to the cell nucleus. These MTs can serve as tracks along which organelles and vesicles are transported either towards or away from the center of the cell. In neurons vesicles are moved along MTs towards a synapse. MTs are the main components of the cores of cilia and flagella. These extensions from the cell surface are used to move fluids and other particles around the cell or the whole cell. Both transport along MTs and ciliary movement are achieved by means of a special class of proteins that bind to the MT surface and are called microtubule associated motor proteins [4]. Another group of MT associated proteins that bind to MTs are called MAPs. These proteins often serve as interconnecting bridges between MTs and they are mainly known as promoters of MT assembly.

The array of MTs surrounding the centrosome is a dynamic structure. MTs are continuously growing and shrinking in random directions. This phenomenon is known as dynamic instability [5]. Net growth or net shrinkage of a single MT is a result of growing and shrinking at the two MT ends. According to observations the transitions between the growing and shrinking phases at a MT end are stochastic. The two ends behave independently of each other: the frequencies of transitions between growing and shrinking and the rates of these processes at both ends are uncorrelated [6]. While the assembly is a linear process the disassembly happens very rapidly.

The microscopic nature of the dynamic instability of MTs

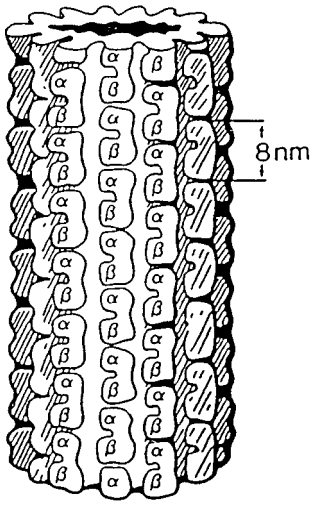

FIG. 1. A schematic drawing of a MT that consists of 13 protofilaments. The tubulin dimers are arranged in a helical manner (from Ref. [3]).

has not been elucidated yet. It is utilized by the cell, for example, in the early phases of cell division. In this period MTs extend from the centrosome in random directions. Those that have completely shrunk are replaced by new ones that start growing from a different nucleation site. In such a way the MTs stochastically probe the whole cellular space in order to eventually become attached to the chromosomes. In [7] it was estimated that a chromosome is attached to a MT within 2 min.

II. GTP HYDROLYSIS AND MODELS OF PROPAGATION OF KINKS ALONG MICROTUBULES

The attachment of a tubulin dimer at a growing MT end is accompanied by the hydrolysis of guanosine 5′ triphosphate (GTP) bound at the exchangeable binding site on the β monomer [8]. Experiments show that the exchangeable GTP hydrolyses very soon after the tubulin binds to the MT. At $p\mathrm{H}=7$ this reaction takes place according to the formula

$$\mathrm{GTP}^{4-}+\mathrm{H_2O}\rightarrow \mathrm{GDP}^{3-}+\mathrm{HPO_4}^{2-}+\mathrm{H}^{+}+\Delta E, \qquad (1)$$

where the released energy ΔE is the same for the hydrolysis of all 5′ triphosphates and amounts to $\Delta E=8.7$ kcal/mol [9].

GTP hydrolysis is a source of energy that is utilized by a MT in ways largely not explained. In [10] the measurements of the standard free energy of the hydrolysis of the nonhydrolysable analogue of GTP, guanylyl-(a,b) -methylene-diphosphate (GMPCPP) are reported. This energy is 5.18 kcal/mol in solution, 3.79 kcal/mol when GMPCPP is bound within a free tubulin molecule, and only 0.9 kcal/mol$=6.25\times10^{-21}$ J when the tubulin is embedded in a MT as a subunit.

It is reasonable to assume that the energies released in the hydrolysis of GTP are in a ratio similar to the ratio between the energies of the GMPCPP hydrolysis. Then the above numbers indicate that most of the energy of the GTP hydrolysis is stored in the assembling MT. It is conjectured that the stored energy has a form of conformational states of the tubulin dimers. The conformational changes of the tubulins after the hydrolysis may cause a mechanical strain that destabilizes MTs. When, due to some other destabilizing event, the MT starts to disassemble, the mechanical strain may be the factor that causes breakage of the bonds between the tubulin subunits, which may result in a partial or overall destruction of the MT [10,11]. It has also been suggested that if the stored mechanical energy is larger than the energy needed for the breakage of the bonds between the tubulin molecules, the surplus can be used to do mechanical work, for example, by coupling disassembly to the vesicle or chromosome movement [12].

However, at least 6.25×10^{-21} J of the energy of the GTP hydrolysis is not stored in a MT. Several groups of researchers put forward a hypothesis that this energy propagates along MTs as a solitary wave. Chou *et al.* [13] showed that kinks and pulses excited, e.g., by the energy freed in the GTP hydrolysis can propagate along MTs due to the coupling between the elastic states of the tubulin dimers. A part of the work presented here follows a paper by Satarić *et al.* [14] in which it is suggested that nonlinear coupling between dielectric and elastic degrees of freedom of tubulin may give rise to kinklike excitations traveling along MT protofilaments.

We can mention two other works by Satarić and coworkers [15,16]. The authors proposed a model of propagation of kinklike torsion waves along MT protofilaments based on a similar equation of motion as in [14]. Using quantum mechanical and nonequilibrium statistical physics methods they attempted to calculate theoretically some physical characteristics of MTs.

In the following sections two models are presented that are mathematically represented by nonlinear partial differential equations that describe appropriate equations of motion. A special class of solutions of these equations are traveling kinks. The first model is a modified version of the model proposed by Satarić *et al.* [14] in which the dynamics of a tubulin dimer is represented by a single (effective) equation of motion derived for the elastic displacement of the dimer. The electric field in the MT that enters into this equation is assumed to be constant. In this paper we modeled the electric field in a MT as a function of the position along the MT. The second model was proposed by Gordon [17] to describe the propagation of stress waves that are coupled to polarization waves in ferroelectric crystals. These waves have the form of kinklike nucleation fronts.

Both models have been modified to study the effect of a collision of the traveling kink with a local defect in a MT. This defect is viewed as a local distortion that can be due to an attached associated protein or a structural discontinuity in the MT. Changing number of protofilaments, extra seams (discontinuity along a MT caused by the mismatch of the rows of tubulin dimers), and point dislocations have all been experimentally observed. The collision with a local impurity may, for example, be a way the energy of the GTP hydrolysis is transferred to another MT through an associated protein. Based on Gordon's model it will be shown that such a collision may be a factor in the MT destabilization or may even cause a complete destruction of a MT.

III. MODEL I: PROPAGATION OF DOMAIN WALLS ALONG MICROTUBULE PROTOFILAMENTS

A. Equation of motion

It has been found in experiments that, like many other biological structures, MTs exhibit pyroelectric and piezoelectric properties that arise as a result of elementary dipole moments carried by their subunits [18]. According to the theoretical work of Fröhlich changes in conformational states (spatial arrangements) of proteins can be induced by redistribution of charges within these polymers [19]. Adopting Fröhlich's concept, in [3] and other related works [20], a model of a MT automaton was proposed based on the assumption that a tubulin molecule can possess two different orientational dipolar states that are coupled to the tubulin conformational states. These states were viewed as two states of an electron that could be localized either towards the α or towards the β monomer and they were termed the α and the β state, respectively.

Following the considerations above we will assume that each tubulin dimer can be in two dipolar states characterized by opposite orientations with respect to the MT axis but the same magnitude of the dipole moment. These states will also be termed the α and the β state and they will be assumed to be coupled to the tubulin conformational states which may

represent different elastic states of tubulin.

According to the model analyzed in this section the coupling between dielectric and elastic degrees of freedom of tubulin is nonlinear. Special solutions of this model are traveling kinklike solitary waves that represent domain walls between two chains of tubulin dimers characterized by different orientation of dipoles and therefore by different elastic states of tubulin. If lateral interactions between the neighboring protofilaments in a MT are neglected, the domain wall propagates along one MT protofilament.

The solitary waves can be excited by the free portion of the energy of the GTP hydrolysis if this amount of energy is sufficiently large to alter the state of a tubulin dimer. Considering only the nearest neighbor dipole-dipole interaction the energy of a tubulin dimer at an assembling MT end is about 10^{-21} – 10^{-20} J [21]. The latter numbers are of the same order of magnitude as the energy freed in the GTP hydrolysis. Hence, this energy may indeed initiate the kink waves traveling along MT protofilaments. In order for the kinks to propagate the dipoles on the tubulin dimers have to be aligned in the same direction, i.e., the MT has to be in a ferroelectric phase [21]. When a MT is in this phase then flipping one dipole can induce flipping of another dipole and so on.

In the model by Satarić *et al.* the energy of an assembly of dipoles placed at discrete sites in a MT protofilament that consists of N tubulin dimers is represented by the following Hamiltonian:

$$H=\sum_{n=1}^{N}\left[\frac{1}{2}M\left(\frac{du_n}{dt}\right)^2+\frac{1}{2}K(u_{n+1}-u_n)^2-\left(\frac{\alpha_2}{2}u_n^2-\frac{\alpha_4}{4}u_n^4\right)-cu_n\right]. \tag{2}$$

In the equation above the variable u_n represents the projection on the protofilament axis of the elastic distortion of the tubulin molecule (different conformation). Describing the dynamics of the tubulin dimers in terms of only one of the variables (elastic state) assumes that the other variable (dipole state) behaves in the same way. Such a situation may occur, for example, if both variables are strongly coupled. The meaning of the terms in Eq. (2) is the following.

$1/2M(du_n/dt)^2$ is the kinetic energy of the tubulin molecule of mass M, $1/2K(u_{n+1}-u_n)^2$ represents the elastic energy that originates from the restoring elastic forces acting between two neighboring dimers. The quartic double well potential energy $V(u_n)=-(\alpha_2/2)u_n^2+(\alpha_4/4)u_n^4$ approximates the average effect of the surrounding dipoles on the dipole at site n. This approximation of the effect of the environment assumes that all dipoles are in their equilibrium positions and they can be either in an α or in a β state, each of which has the same energy. The dipole states of each tubulin in the α and β state can then be represented by two dipoles, which are aligned along the MT protofilament axis and point in opposite directions. In [21] calculations are presented according to which a MT may undergo a dielectric transition from a ferroelectric to a paraelectric phase. Assuming that this transition has characteristics of a second order phase transition, α_4 is a positive constant and $\alpha_2=a_2(T_c-T)$, where $a_2>0$ and T_c is the critical temperature

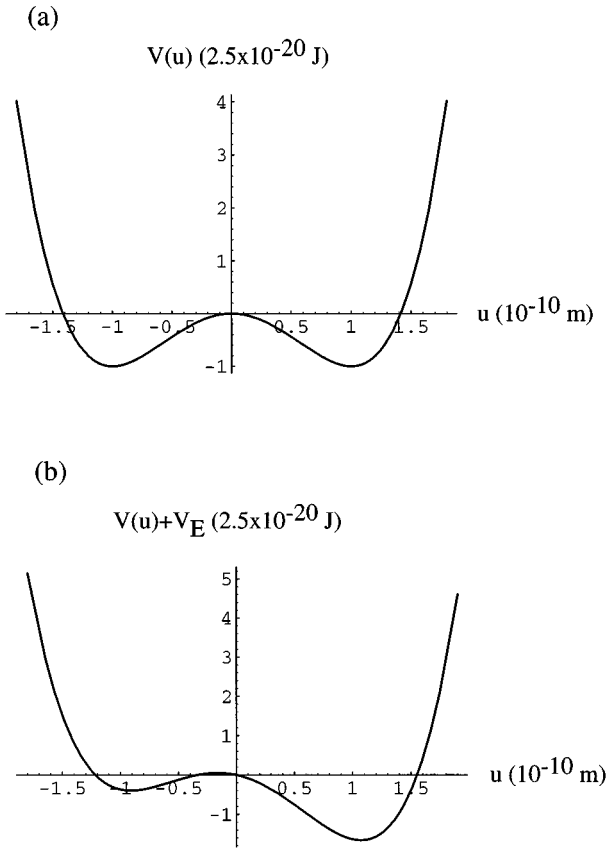

FIG. 2. The local potential energy at a site n in a MT protofilament when the MT is in a ferroelectric phase. (a) $V(u_n)$, (b) $V(u_n)+V_E$.

of the transition. Under these assumptions below T_c the potential energy $V(u_n)$ exhibits two symmetric local minima at $u_n=\pm(\alpha_2/\alpha_4)^{1/2}$ for which $V_{\min}=-\alpha_2^2/(4\alpha_4)$ and a maximum at $V(0)=0$ [Fig. 2(a)].

The last term $-cu_n$ in Eq. (2) accounts for the effect of an electric fields to which the chain of dipoles in the protofilament can be exposed. The total electric field E at site n of the protofilament produces potential energy $V_E=-cu_n=-q_{\text{eff}}Eu_n$, where q_{eff} is the effective charge of the nth tubulin dimer. The addition of V_E to the quartic double-well potential energy $V(u_n)$ results in an asymmetric function with two local minima and one local maximum. One of the two minima corresponds to a lower energy, which means that the two dipole states are not equivalent but the state that is oriented in the direction of the electric field has a lower energy and thus it is energetically more favorable for the tubulin molecule to be in this state [Fig. 2(b)].

A situation can be also considered when the dipoles on the tubulins are not parallel to the MT axis but tilted by a certain angle with respect to it. If the dipoles are tilted by different angles in the α and in the β state then the two states do not have the same energy. However, dipoles tilted with respect to an axis can be viewed as dipoles parallel to this axis that are subjected to an effective electric field [22]. (Consider a dipole that can be in one of two orientational states that, when projected on a chosen axis, point in opposite directions. A Hamiltonian of an assembly of such dipoles can be written as a sum of the Hamiltonian of an as-

sembly of dipoles in which each dipole can be in one of two orientational states that are parallel to this axis and an effective electric field. This electric field is a function of the interaction energies between the dipoles.) Then in Eq. (2) the potential energy $V(u_n)$ would be the same as for the case when the dipoles are parallel to the MT axis and the effect of the effective electric field could be included in the term $-cu_n$. Thus, if the dipoles on the tubulin dimers are tilted by different angles with respect to the MT axis then the kinks that represent switching from the α to the β state or *vice versa* (depending on which is energetically more favorable) can form even without the presence of external electric fields.

In order to derive a realistic equation of motion, the effect of the medium surrounding a MT has to be taken into account. Cellular MTs are imbedded in cytosol, which is a water solution of various ions. Ions and polar water molecules can affect the electrostatic interactions between the dipoles on the dimers and they can also act as a viscous medium and damp the motion of the dimers [14]. The damping effect can be represented by a viscous force

$$F_v = -\gamma \frac{\partial u_n}{\partial t}, \tag{3}$$

where γ is the damping coefficient.

The above force and the Hamiltonian (2) lead in the continuum approximation to the following equation of motion for the displacement variable $u(x,t)$:

$$M\frac{\partial^2 u(x,t)}{\partial t^2} - KR_0^2 \frac{\partial^2 u(x,t)}{\partial x^2} - \alpha_2 u(x,t) + \alpha_4 u(x,t)^3 + \gamma \frac{\partial u(x,t)}{\partial t} - q_{\text{eff}} E(x) = 0\,. \tag{4}$$

Here, $R_0 = 8\times 10^{-9}$ m is the equilibrium distance between two neighboring tubulin molecules and the rest of the parameters in Eq. (4) can be determined as follows [14]:

Taking the molecular weight of each tubulin monomer as 55 kilodaltons, the mass M is 1.83×10^{-22} kg. The product KR_0^2 can be written in terms of the velocity of longitudinal sound v_0: $KR_0^2 = M\omega^2 R_0^2 = Mv_0^2$. The speed of sound in a MT was approximately calculated in [23]. This calculation yielded $v_0 \approx 610\ \text{ms}^{-1}$. However, in the numerical calculations presented below the value $v_0 = 1700\ \text{ms}^{-1}$ has been used since it gave more physical results. The latter number is the velocity of sound measured in DNA [24].

The coefficients α_2 and α_4 have not been determined for a MT so far. For the purposes of the analysis presented here we used the parameters experimentally measured in inorganic crystals, which are known to form ferrodistortive domain walls. Based on experimental data for the crystal $Pb_5Ge_3O_{11}$ below the critical temperature the estimated values of these parameters are $a_2 = 10\ \text{Jm}^{-2}\text{K}^{-1}$ and $\alpha_4 = 1.6\times 10^{24}\ \text{Jm}^{-4}$ [25]. If a MT is in the ferroelectric phase, then the critical temperature T_c can be approximately taken as 350 K and T is body temperature, i.e., 310 K. This yields $\alpha_2 = 400\ \text{Jm}^{-2}$.

To determine the damping coefficient γ, the tubulin dimer can be considered a sphere of radius $R_s = 4\times 10^{-9}$ m and mass M that is moving in a fluid of viscosity η. The drag force exerted by the fluid on the sphere is

$$F_v = -6\pi R_s \eta \frac{du}{dt} = -\gamma \frac{du}{dt}. \tag{5}$$

Assuming that a MT is mainly surrounded by water molecules η can be approximated by the viscosity of water at body temperature. Using $\eta = \eta_{\text{water}} = 6.9\times 10^{-4}\ \text{kgm}^{-1}\text{s}^{-1}$ gives for the damping coefficient $\gamma = 6\pi R_s \eta$ the value $5.2\times 10^{-11}\ \text{kg s}^{-1}$.

B. Electric field of a microtubule

The electric field $E(x)$ in a MT may be due to the external fields produced by other cellular structures or other MTs and also by the MT itself. The existence of the intrinsic field generated by a MT is indicated by the observation of the so-called ''clear zone'' [20]. This is a space in the shape of a tube that surrounds a MT and is 5–10 nm wide. According to experiments, organelles, the cytoplasmic ground substance or any other material normally seen throughout the cell, are very seldom present in this zone. Another indication about the electromagnetic nature of MTs comes from the experiments reported in [26] in which MTs aligned along electric fields of the order of magnitude $1\ \text{Vm}^{-1}$ and magnetic fields of intensity 0.02 T.

However, the exact distribution of charges in the tubulin molecules bound in a MT is not known. Therefore, an approximation was chosen to calculate the electric field of a MT. The charge distribution was represented by a net positive point charge placed at the protofilament axis at one protofilament end and net negative point charge at its other end. The electric field $E(x)$ along the axis of the protofilament on which the kink propagates was assumed to be produced by the remaining 12 protofilaments in the MT (the MT was assumed to consist of 13 protofilaments). The corresponding formula is

$$E(x) = \sum_{i=1}^{12} \frac{q_{\text{eff}}}{4\pi\epsilon_0\epsilon_r}\left\{ \frac{L/2+x}{[d_i^2 + (L/2+x)^2]^{3/2}} + \frac{L/2-x}{[d_i^2 + (L/2-x)^2]^{3/2}} \right\}, \tag{6}$$

where $q_{\text{eff}} = 1.602\times 10^{-19}$ C, L is the MT length, ϵ_0 is the permittivity of vacuum, ϵ_r is relative permittivity of a MT, and $d_i = 2R\sin(i\alpha/2)$ is the distance of the axis of the ith protofilament from the axis of the 13th protofilament. In the latter expression $R = 10.4\times 10^{-9}$ m is the distance of the charges from the center of the MT and $\alpha = 2\pi/13$ is the angle subtended by each tubulin dimer. R was obtained by approximating a tubulin dimer as a cylinder whose cross-sectional area has a radius $r = 2.5\times 10^{-9}$ m (and a height $R_0 = 8\times 10^{-9}$ m). The dielectric constant ϵ_r is not known for MTs. But because MTs are mainly surrounded by water molecules, this parameter can be approximated by the permittivity of free water, which, depending on frequency, ranges at body temperature from about 70 (static value) to about 4 (in

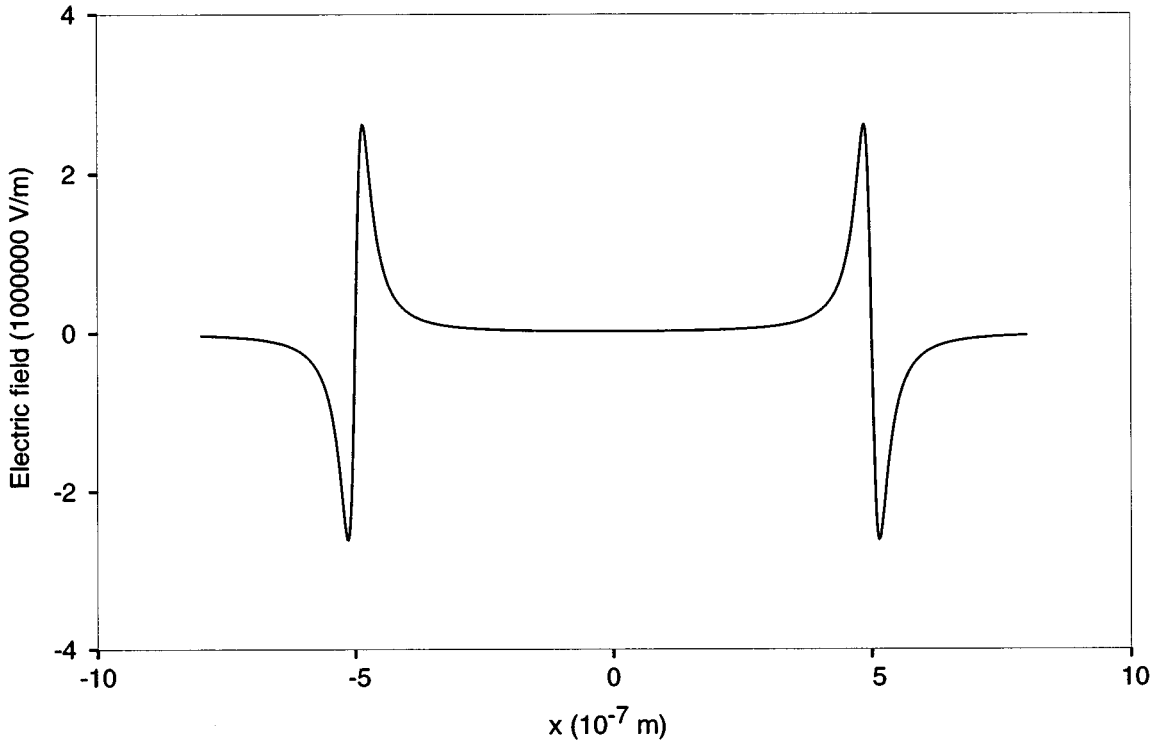

FIG. 3. The electric field generated along the axis of a MT protofilament by the charges of equal magnitudes and opposite signs placed at the ends of the axes of the remaining 12 protofilaments. Each protofilament consists of 125 dimers.

the infinite limit) [27]. The electric field (6) is plotted for the parameters given above, $\epsilon_r=1$ and a 10^{-6} m long MT (125 dimers) in Fig. 3.

C. Analytical solution (constant electric field along a microtubule)

Equation (4) can be solved analytically for a constant electric field [14]. In order to find a solution in the form of a traveling wave that moves at a constant velocity v, a moving coordinate $\xi=\xi(x-vt)$ can be introduced as follows:

$$\xi=\left[\frac{|\alpha_2|}{M(v_0^2-v^2)}\right]^{1/2}(x-vt). \tag{7}$$

The partial differential equation (4) reduces then to an ordinary differential equation

$$\frac{d^2\psi}{d\xi^2}+\rho\frac{d\psi}{d\xi}-\psi^3+\psi+\sigma=0, \tag{8}$$

where

$$\rho=\frac{v\gamma}{[M\alpha_2(v_0^2-v^2)]^{1/2}},\quad \sigma=\alpha_4^{1/2}\alpha_2^{-3/2}qE \tag{9}$$

and

$$\psi(\xi)=\frac{u(\xi)}{u_0},\quad u_0=\left(\frac{\alpha_2}{\alpha_4}\right)^{1/2}. \tag{10}$$

The traveling kink wave solution of (8) is listed in [28]. The solution that corresponds to a kink moving with a velocity $v>0$ is

$$\psi(\xi)=\psi_2+\frac{\psi_1-\psi_2}{1+e^{\xi(\psi_1-\psi_2)/\sqrt{2}}}, \tag{11}$$

where

$$\psi_1=\frac{2}{\sqrt{3}}\cos\left\{\frac{1}{3}\arccos\left[\frac{3qE}{2\alpha_2}\left(\frac{3\alpha_4}{\alpha_2}\right)^{1/2}\right]\right\}, \tag{12}$$

$$\psi_2=\frac{2}{\sqrt{3}}\cos\left\{\frac{2\pi}{3}+\frac{1}{3}\arccos\left[\frac{3qE}{2\alpha_2}\left(\frac{3\alpha_4}{\alpha_2}\right)^{1/2}\right]\right\}. \tag{13}$$

The maximum value of the electric field plotted in Fig. 3 is $E_{\max}=2.62\times10^6\ \mathrm{V\,m^{-1}}$. For this value the variable $\delta=(3qE/2\alpha_2)(3\alpha_4/\alpha_2)^{1/2}=0.000115$. Hence $\psi_1-\psi_2$ is positive and the kink (11) is a domain wall between two states $\psi=\psi_1$ when $\xi\to-\infty$ and $\psi=\psi_2$ when $\xi\to\infty$, traveling to the right. This solution is consistent with the potential energy $V(u)+V_E$ plotted in Fig. 2(b). The state of the variable $u=u_0\psi$ changes from a negative to a positive value as the domain wall moves towards the right boundary.

Since the argument δ is very small for the values of the electric field along a MT obtained from Eq. (6), ψ_1 and ψ_2 can be safely expanded with respect to δ around 0. Keeping only terms up to the first order in δ results in the following approximate expression for the kink wave:

$$u(\xi)=\left(\frac{\alpha_2}{\alpha_4}\right)^{1/2}\left[-1+\frac{\delta}{3^{3/2}}+\frac{2}{1+e^{\sqrt{2}\xi}}\right]. \tag{14}$$

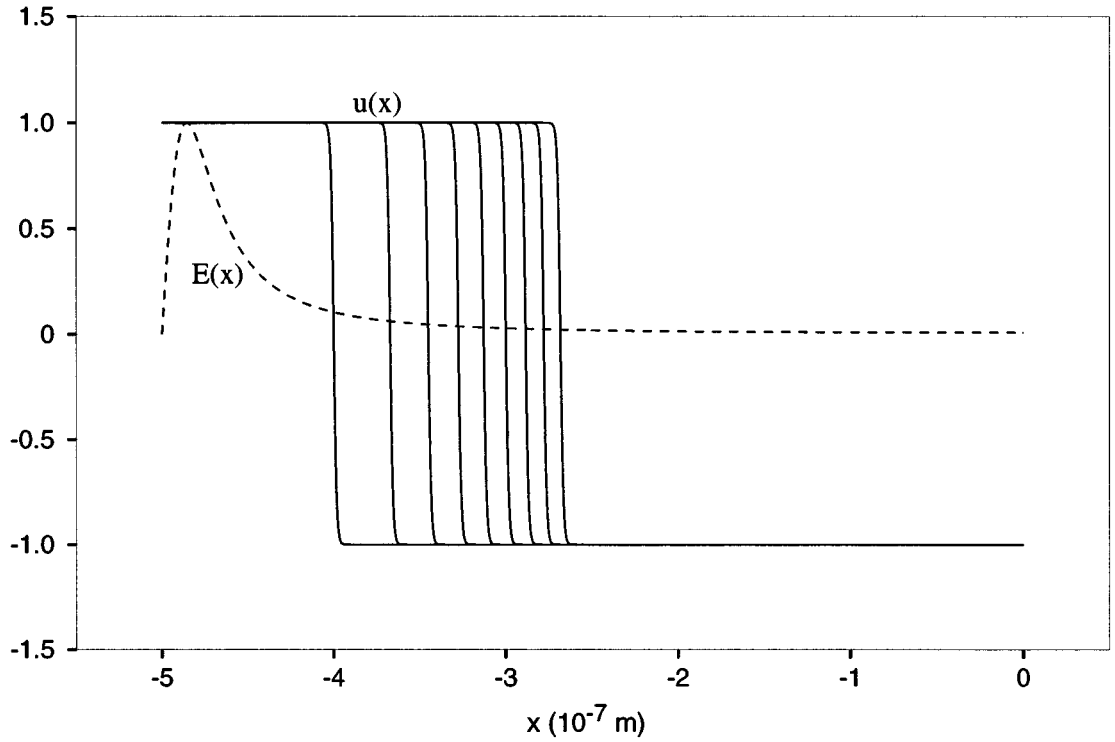

FIG. 4. A kink wave moving along a section of a MT that is 125 dimers long. The wave is exposed to a decreasing electric field of the MT. The electric field is plotted in units $2.62\times10^{6}\ \mathrm{V\,m^{-1}}$ and the displacement $u(x)$ is in units 1.58×10^{-11} m. The time interval between two successive waves is $\Delta t=3.38\times10^{-7}$ s.

The latter equation is valid with very good accuracy and it was used in the numerical simulations presented below.

The kink solution of Eq. (8) is obtained if the following condition is satisfied [14,28]:

$$\frac{v\gamma}{[\alpha_2 M(v_0^2-v^2)]^{1/2}}=-\sqrt{6}\cos\left\{\frac{4\pi}{3}+\frac{1}{3}\arccos\left[\frac{3qE}{2\alpha_2}\left(\frac{3\alpha_4}{\alpha_2}\right)^{1/2}\right]\right\}. \quad (15)$$

Equation (15) determines the velocity of the kinklike solitary wave. Solving Eq. (15) for the values of the parameters α_2, α_4, γ, M, and $q=q_{\mathrm{eff}}$ given earlier and maximum of the electric field $E=E_{\max}=2.62\times10^{6}\ \mathrm{V\,m^{-1}}$ yields $v=1.24\ \mathrm{m\,s^{-1}}$. This number is much smaller than the velocity of phonons $v_0=1700\ \mathrm{ms^{-1}}$. Due to this v^2 in the numerator of the left-hand side of Eq. (15) can be neglected and the right-hand side can be expanded with respect to the small argument δ. The resulting approximate formula for v is

$$v=\frac{3v_0}{\gamma\alpha_2}\left(\frac{M\alpha_4}{2}\right)^{1/2}qE=\frac{3v_0}{\gamma a_2(T_c-T)}\left(\frac{M\alpha_4}{2}\right)^{1/2}qE. \quad (16)$$

The equation above shows how the velocity of kinks depends on the model parameters. For fixed T (body temperature) varying the critical temperature T_c varies the velocity of the domain walls. Clearly, v also changes when the magnitude of the electric field along the MT changes. Since v depends on E linearly, stronger fields produce faster moving kinks and *vice versa*. The value of E can be altered due to several factors: subjecting a MT to external cellular electric fields, varying the MT length [according to the approximation (6) longer MTs generate smaller electric fields and *vice versa*]; ϵ_r may change due to the changes of ionic concentration of the surrounding cytosol, conformational changes of tubulin, or the presence of different tubulin isotypes; screening caused by other charges within the tubulin molecule can substantially lower the value of the intrinsic electric field of a MT.

The kinklike domain walls can be viewed as bits of information propagating along MTs [29]. Due to the coupling between dielectric and elastic degrees of freedom of tubulin this information can be coupled to mechanical events. For example, such kinks may be involved in the movement of motor proteins. If a kink arrives at the other MT end it may weaken the lateral bonds between neighboring tubulins due to the change of the tubulin conformational state. This may cause dissociation of a tubulin dimer in the MT disassembly.

D. Numerical solution (electric field changing as a function of position along a microtubule)

In this section and the following section we present numerical solutions of Eq. (4) under the assumption that the electric field E changes along a MT according to formula (6) using the approximate analytical solution (14) as the initial condition. A sample calculation is given in Fig. 4, which shows a kink wave moving on a section of the MT protofilament along which the intrinsic electric field of the MT decreases. At time $t=0$ the center of the kink is positioned at $x=-4\times10^{-7}$ m. At this point the magnitude of the electric field is $E=274\,000\ \mathrm{V\,m^{-1}}$ and the corresponding initial ve-

locity obtained from formula (16) is $0.13\,\mathrm{m\,s^{-1}}$. The time interval between two successive waves is $\Delta t = 3.38\times10^{-7}$ s.

As is clear from the figure the kink decelerates. During the total time of simulation $T = 2.7\times10^{-6}$ s the domain wall moves a distance $D = 1.32\times10^{-7}$ m, which is about 16 tubulin dimers. The velocity of the kink at the end of the simulation was calculated approximately as $\Delta d_{\mathrm{end}}/\Delta t = 0.0289\,\mathrm{m\,s^{-1}}$, where Δd_{end} is the distance between the last two plotted waves. To compare the numerical solution with the analytical solution the value of the electric field in the center of the interval Δd_{end} ($60\,000\,\mathrm{V\,m^{-1}}$) was substituted into Eq. (16), which yielded $v = 0.0285\,\mathrm{m\,s^{-1}}$.

Similar analysis was done for a kink wave moving on a section of the MT along which the electric field increases. It was found that the velocity of the kinks also increased and was consistent with the formula (16). Thus, it can be concluded that the waves move at a velocity that is proportional to the value of the electric field as was also obtained analytically.

The results above imply that the velocity of the kinks is the lowest at the center of a MT since the electric field is the lowest at this point. At the center of a MT that is 125 dimers long the magnitude of the electric field is $E(0) = 23\,000\ \mathrm{V\,m^{-1}}$. The corresponding velocity from Eq. (16) is $v(0) = 0.0109\,\mathrm{m\,s^{-1}}$. In the center of a MT that consists of protofilaments composed of 1000 dimers the electric field is $360\,\mathrm{V\,m^{-1}}$ and the velocity is $v(0) = 0.000171\,\mathrm{m\,s^{-1}}$. It should be realized that the calculated velocities will be almost two orders less if the static value of the relative permittivity (70) is substituted into Eq. (6). Screening by other charges in the tubulin molecules may considerably decrease the magnitude of the electric field and consequently the velocities of the kink waves as well.

We can see whether the velocities considered above could be related to the dynamical processes associated with MTs: In [30] the measured rates of growth of MTs were in the range 1.6–2.3 μm/min=40–65 dimer/s and the rates of shortening were 10 times higher. As mentioned earlier the cytoplasmic transport along MTs is achieved by means of motor proteins attached to MTs. These are divided into two main groups, kinesins and dyneins. Kinesin purified from squid axons was observed to move MTs at a velocity $0.5\ \mu\mathrm{m\,s^{-1}}$. The rates associated with cytoplasmic dynein were measured in the range $1.25–2\ \mu\mathrm{m\,s^{-1}}$. It could be mentioned that the latter rates are the same as the rates of the poleward movement of chromosomes in prometaphase of cell division [4]. The measured rates of movement associated with flagellar dynein purified from sea urchin and *Chlamydomonas* were about $10\ \mu\mathrm{m\,s^{-1}}$. These numbers show that there is some agreement between the experimental measurements and the calculated velocities of the kinks.

E. Effects of impurity potentials

The mathematical modeling presented in this paper is mainly focused on the effect of a collision of the traveling kinklike solitary wave with an impurity in a MT. In this model the impurity was viewed as a source of localized potential energy, which was chosen to have the form of the Gaussian function below

$$V(x) = V_0 \sum_{n=1}^{N} e^{-\beta\{x-[x_d+(n-1)a_n]\}^2}. \tag{17}$$

In the equation above, N is the number of defects along a MT protofilament, x_d is the location of the first impurity, a_n is the distance between two impurities, β is a constant that determines the steepness of the Gaussian bump or well, and V_0 is the amplitude of the potential energy. The force produced by the potential energy (17) is

$$\frac{dV(x)}{dx} = -2V_0\beta \sum_{n=1}^{N} \{x-[x_d+(n-1)a_n]\} e^{-\beta\{x-[x_d+(n-1)a_n]\}^2}. \tag{18}$$

This force was added to the left-hand side of Eq. (4).

Figure 5 shows the motion of a kink wave on a section of the MT protofilament where the background electric field $E(x)$ from the surrounding 12 protofilaments decreases and at time $t = 0$ s a localized potential energy $V(x)$ centered at $x_d = -3.7\times10^{-7}$ m is switched on. The kink starts moving at a point $x_0 = -4.0\times10^{-7}$ m with a velocity $v_0 = 0.13\,\mathrm{m\,s^{-1}}$ and the time interval between two successive waves is $\Delta t = 1.35\times10^{-7}$ s. The potential energy function is a bump with parameters $\beta = 10^{17}\ \mathrm{m^{-2}}$ and the amplitude $V_0 = 1.00\times10^{-22}$ J, which corresponds to the maximum amplitude of the local force $\pm 2.71\times10^{-14}$ N.

As can be seen, in the presence of the localized potential energy $V(x)$ the velocity of the kink wave changes more rapidly compared to the case when only the electric field is present. When the kink approaches the defect, its velocity decreases because the local force produced by the impurity is negative. When the kink moves away from the center of the defect, its velocity increases since the defect generates a positive force. Eventually the wave moves with a steadily decreasing speed due to the smoothly decreasing electric field $E(x)$. The overall distance traveled by the wave when the local potential energy is switched on is smaller than the distance the kink moves in the same amount of time only on the background of the electric field. This is indicated by the difference between the last solid line and the dotted line, which represents a kink that traveled only on the background of the changing electric field.

Increasing the amplitude of the local potential barrier results in a greater delay of the kink and when the amplitude reaches a critical value the kink will come to a complete stop. This is illustrated in Fig. 6 where the kink wave is stopped by a bump centered at $x_d = -3.7\times10^{-7}$ m. The amplitude of the bump is 1.00×10^{-21} J and the corresponding maximum amplitude of the local force is $\pm 2.71\times10^{-13}$ N (10 times larger than in the previous case). The absolute value of the minimum of the local force is larger than the force due to the electric field at the corresponding point $[q_{\mathrm{eff}}E(-3.72\times10^{-7}\ \mathrm{m}) = (1.602\times10^{-19})(1.74\times10^{6})\ \mathrm{N} = +2.78\times10^{-14}\ \mathrm{N}]$ and since the two forces have opposite signs the kink is stopped.

The width of the kinks shown in Figs. 4–6 is about one tubulin dimer. When the value of the sound velocity $v_0 = 610\,\mathrm{m\,s^{-1}}$ is used, this reduces the kink width to about one-third of the tubulin dimer, which is not very realistic.

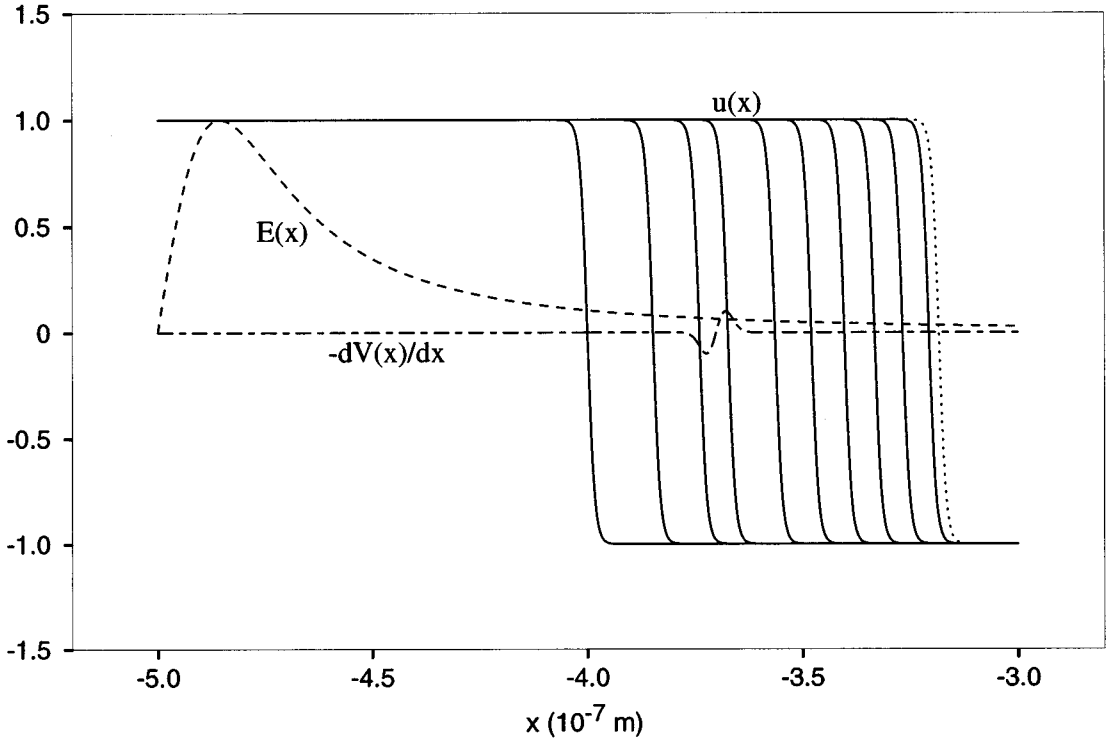

FIG. 5. A kink wave traveling on a section of a MT protofilament along which the electric field decreases. The protofilament contains a defect that is represented by a localized potential energy centered at a point $x_d = -3.7\times10^{-7}$ m. The amplitude of the local potential energy is 1.00×10^{-22} J and the length of the MT protofilaments is 125 dimers. The dotted line shows how far the kink would travel if there was no defect. The electric field is plotted in units 2.62×10^{6} V m^{-1}, the local force is in units 2.71×10^{-13} N, and the kink wave is in units 1.58×10^{-11} m.

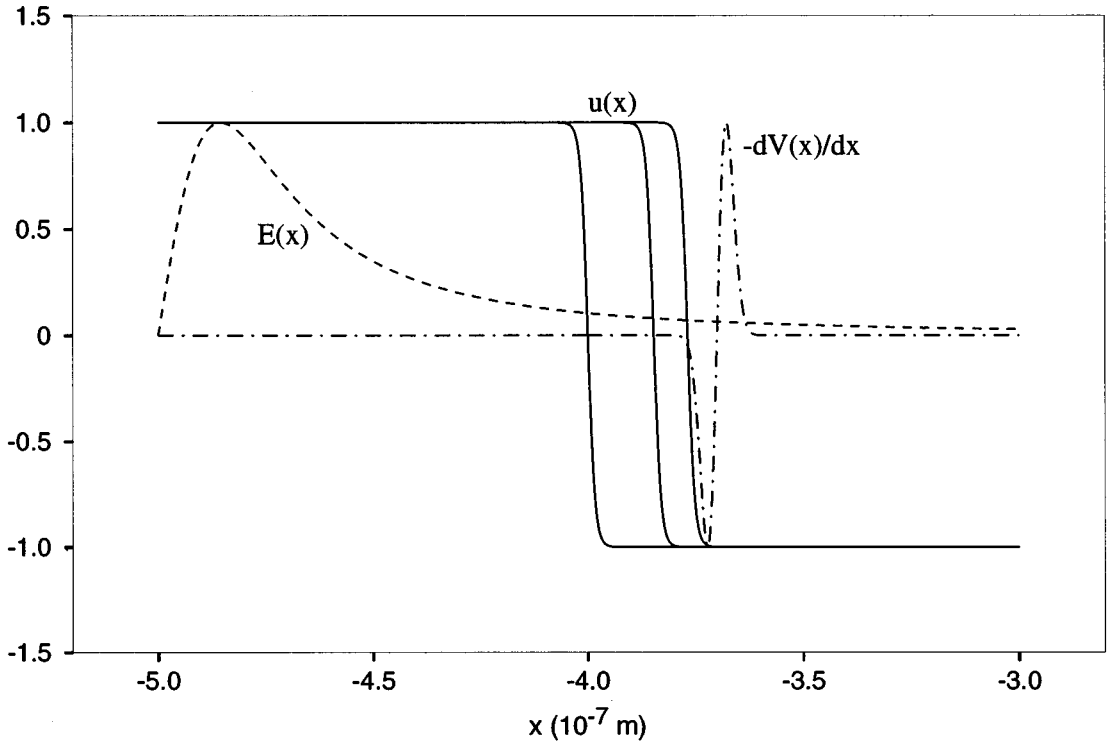

FIG. 6. When the defect in a MT produces a sufficiently large potential barrier, the kink wave is stopped. In this case the amplitude of the potential energy due to the defect is 1.00×10^{-21} J and it is located at $x_d = -3.7\times10^{-7}$ m in a MT protofilament that is 125 dimers long. The units for all curves are the same as in Fig. 5.

This means that using $610\,\mathrm{m\,s^{-1}}$ as the value of the velocity of sound in MTs within this model would require an adjustment of other model parameters. On the other hand, if it is assumed that the rest of the model parameters are correct then the value $610\,\mathrm{m\,s^{-1}}$ for the velocity of sound in MTs has to be corrected.

IV. MODEL II: PROPAGATION OF NUCLEATION FRONTS ON MICROTUBULES

The second model of propagation of kinklike solitary waves in MTs analyzed here is based on the works [17] and [31] in which is proposed a model of the interface motion in ferroelectric crystals. In [17] the Landau-Ginzburg-type free energy expansion is postulated in the following form:

$$F=F_0+\frac{1}{2}AP^2-\frac{1}{4}BP^4+\frac{1}{6}CP^6-\frac{1}{2}e\sigma P^2-\frac{1}{2}s_0\sigma^2+\frac{D}{2}\left(\frac{\partial P}{\partial x}\right)^2, \tag{19}$$

where P is polarization and σ is mechanical stress that couples to P due to the piezoelectric effect. Coupling between P and σ is expressed by the term $\frac{1}{2}e\sigma P^2$, where e is an elastic constant. The parameter s_0 is related to the velocity of sound v_0 and the density ρ of the elastic medium through $v_0=(\rho s_0)^{-1/2}$. Without the terms containing σ, the free energy (19) describes a first order phase transition in uniaxial proper ferroelectrics. The coefficient A is defined as $A=a(T_0-T)$, where T_0 is the transition temperature at which the paraelectric phase loses its stability (see Fig. 12, of [32]), B and C are positive constants. The term $(D/2)(\partial P/\partial x)^2$ represents the nonuniformity energy that exists in the transition regions between domains in which the direction of polarization is different and $D>0$ [33].

The time evolution of the order parameter P can be derived using the time dependent Landau-Ginzburg equation [34],

$$\frac{\partial P}{\partial t}=-\Gamma\frac{\delta F}{\delta P}, \tag{20}$$

where Γ is the Landau-Khalatnikov damping coefficient. Substituting Eq. (19) into Eq. (20) and performing the variational derivative $\delta F/\delta P$ gives the following equation:

$$\frac{\partial P}{\partial t}+\Gamma(AP-BP^3+CP^5-e\sigma P)-\Gamma D\frac{\partial^2 P}{\partial x^2}=0\,. \tag{21}$$

The second equation for σ and P can be found from the coupling of both variables to the mechanical deformation ϵ, which is equal to

$$\epsilon=-\frac{\partial F}{\partial\sigma}=\frac{1}{2}eP^2+s_0\sigma. \tag{22}$$

Here, $\epsilon=\partial u/\partial x$ is the strain tensor component corresponding to σ. Hence, it satisfies the wave equation of an elastic medium with a density ρ:

$$\rho\frac{\partial^2\epsilon}{\partial t^2}=\frac{\partial^2\sigma}{\partial x^2}. \tag{23}$$

After substituting Eq. (22) into Eq. (23) the second equation for coupled polarization and mechanical stress is obtained:

$$\frac{\rho e}{2}\frac{\partial^2}{\partial t^2}P^2=\left(\frac{\partial^2}{\partial x^2}-\rho s_0\frac{\partial^2}{\partial t^2}\right)\sigma. \tag{24}$$

To find the solutions of the system of coupled equations (21) and (24) in the traveling wave form the traveling coordinate $\xi=x-vt$ can be introduced. Then Eq. (24) can be integrated, which yields

$$\frac{\rho e}{2}v^2P^2-(1-\rho s_0v^2)\sigma=c_1\xi+c_0\,. \tag{25}$$

In Eq. (25), c_1 and c_0 are integration constants. If it is assumed that $c_1=c_0=0$ (the solutions for c_1 and c_0 nonzero were studied, e.g., in [35]) and Eq. (25) is substituted into Eq. (21), the following ordinary differential equation results for P:

$$\Gamma D\frac{d^2P}{d\xi^2}+v\frac{dP}{d\xi}-\Gamma(AP-\widetilde{B}P^3+CP^5)=0\,, \tag{26}$$

where

$$\widetilde{B}=B+\frac{\rho e^2v^2}{2(1-\rho s_0v^2)}. \tag{27}$$

The solution of Eq. (26) is a traveling kink wave,

$$P=\frac{P_f}{\sqrt{2}}\left[1+\tanh\left(\frac{\xi}{2\Delta}\right)\right]^{1/2}, \tag{28}$$

where

$$P_f^2=\frac{\widetilde{B}}{2C}\left[1+\left(1-\frac{4AC}{\widetilde{B}^2}\right)^{1/2}\right], \tag{29}$$

$$\Delta=\left[\frac{3D}{4(\widetilde{B}P_f^2-A)}\right]^{1/2}, \tag{30}$$

and

$$v=\frac{2}{3}\Gamma\Delta(4A-\widetilde{B}P_f^2)=\Gamma\widetilde{B}\left(\frac{D}{6C}\right)^{1/2}\frac{8AC/\widetilde{B}^2-1-\sqrt{1-4AC/\widetilde{B}^2}}{(1-2AC/\widetilde{B}^2+\sqrt{1-4AC/\widetilde{B}^2})^{1/2}}. \tag{31}$$

We assume that a defect in a MT can be represented as a local fluctuation of the density of the medium, which was chosen to have a form similar to Eq. (17):

$$\rho(x)=\rho_0\left(1+\rho_r\sum_{n=1}^{N}e^{-\beta\{x-[x_d+(n-1)a_n]\}^2}\right), \tag{32}$$

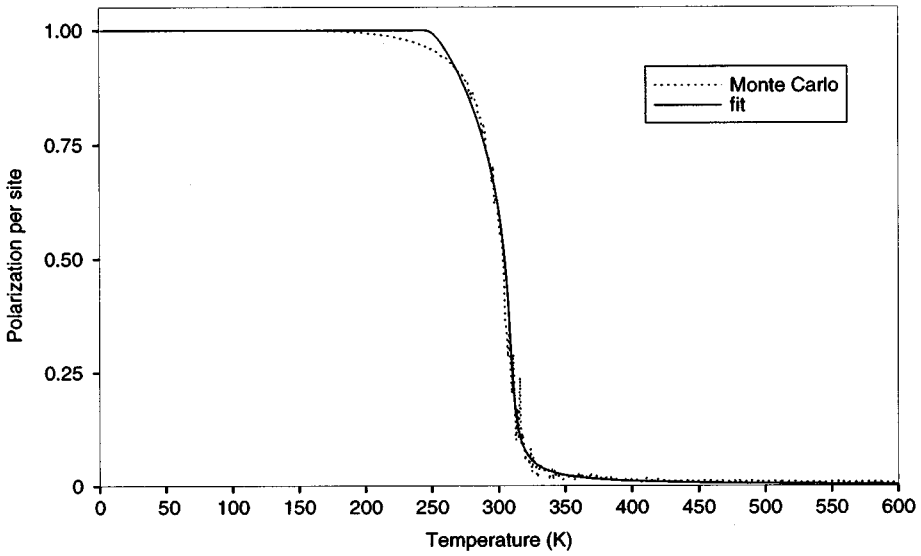

FIG. 7. Relative polarization in a MT with the A lattice and size 13×3000 for $Q=12\times10^{-56}\ \mathrm{C^2\,m^2}$ (dotted line), and the curve calculated by finding the roots of Eq. (33) (solid line).

where $\rho_0=$ const is the density in the medium when no defect is present and ρ_r is the dimensionless amplitude of the density inhomogeneity.

The system of partial differential equations (21) and (24) in which the density of the medium changes along a MT according to Eq. (32) was solved numerically. As initial conditions were chosen the solutions for constant density $\rho=\rho_0$ that were obtained from Eq. (28) for P and by combining Eqs. (28) and (25) for σ. The value of ρ_0 was calculated as $M/\Delta V$, where M and ΔV were assumed to be the same as in Sec. III. The velocity of sound was also chosen the same as in Sec III, i.e., $v_0=1700\ \mathrm{m\,s^{-1}}$.

The rest of the constants that appear in Eqs. (21) and (24) are not known for a MT. However, the parameters A, B, C, and D could be estimated by fitting curves of polarization of a MT as a function of temperature, which were discussed, e.g., in [21]. The curve that was used for the estimate is represented by the dotted line in Fig. 7. The solid line is the fit. The dotted line is a normalized plot of polarization per site (sum of all dipole moments divided by the sum of magnitudes of all dipoles) obtained by applying the classical Monte Carlo procedure to the system of dipoles in a MT that consists of 13 protofilaments and 3000 rows. The dipoles in both the α and the β state were assumed to be parallel to the MT axis and only the nearest-neighbor interactions were taken into account. The sites at which the dipoles are centered (centers of the tubulin dimers) formed a lattice of the so-called A type (the A-type arrangement of tubulin molecules in a MT can be seen in Fig. 1. Another possible arrangement of the tubulin dimers in a MT is B type. Both arrangements are hexagonal and they differ by the amount of longitudinal shift between two neighboring protofilaments [1,36].)

The fit was calculated by adjusting the coefficients in the following equation:

$$0=a_2^t(T-T_c)P_t+A_4^tP_t^3+A_6^tP_t^5-E-Nk_BT\frac{\partial S_{1/2}}{\partial P_t}. \tag{33}$$

Equation (33) was obtained by taking the derivative of free energy with respect to the total polarization P_t (sum of all dipole moments) and setting the resulting expression equal to 0. In this equation E is an electric field that is parallel to the MT axis, $S_{1/2}$ is the entropy of the ensemble of spins whose projections on the z axis can have two values $\pm1/2$, N is the number of spins, and k_B is Boltzmann's constant. $S_{1/2}$ is given by the formula [37]

$$S_{1/2}=Nk_B\left[\ln N-\frac{1+2m}{2}\ln\frac{N}{2}(1+2m)-\frac{1-2m}{2}\ln\frac{N}{2}(1-2m)\right], \tag{34}$$

where m is one-half of the relative polarization. Since Eq. (34) is in terms of m, Eq. (33) had to be expressed in terms of m as well, which required a straightforward manipulation. The coefficients A_{2i}^t, which were obtained from the fit shown in Fig. 7, were transformed into coefficients that correspond to the variable dipole moment (polarization) per site according to the identity

$$A_k^tP_t^{k-1}=\left(\frac{P_t}{N}\right)^{k-1}N^{k-1}A_k^t, \tag{35}$$

where $P=P_t/N$ is the dipole moment per site and $A_k=N^{k-1}A_k^t$ are the corresponding coefficients. Their values are

$$a_2=a=1.14\times10^{32}\ \mathrm{N\,C^{-2}\,m^{-1}\,K^{-1}}, \tag{36}$$

$$A_4=B=3.41\times10^{85}\ \mathrm{N\,C^{-4}\,m^{-3}}, \tag{37}$$

$$A_6=C=8.12\times10^{139}\ \mathrm{N\,C^{-6}\,m^{-5}}. \tag{38}$$

The parameter D was estimated on the basis of the classical interaction energy between two dipoles. If the angle between two dipoles at the interface between two domains with different orientation of dipoles is assumed to be small then D can be approximated by

$$D=\frac{1}{2\pi\epsilon_0\epsilon_rR_0}=3.21\times10^{16}\ \mathrm{N\,C^{-2}\,m}. \tag{39}$$

All parameters above were calculated for the value of the relative permittivity $\epsilon_r=70$ (static value for free water), the magnitude of the tubulin dipole moment $2.90\times10^{-27}\ \mathrm{C\,m}$ and $N=39\,000$. The fit was obtained for the electric field set to $3.5\times10^5\ \mathrm{V\,m^{-1}}$.

It should be noted that the free energy (19) has the units of energy per unit volume. However, the parameters A, B, C and D are derived from an expansion that has the units of energy and for the variable dipole moment per site they correspond to energy per site. In order to have the right dimensions all terms in Eq. (19) except for the term $1/2 s_0 \sigma^2$ have to be divided by the volume of a tubulin dimer. The same result can be achieved by deriving such parameters A, B, C, and D that correspond to the variable dipole moment per unit volume. This can be done by replacing N with $N\Delta V$ in Eq. (35).

A. Numerical results

1. Second order phase transition

According to our analysis the dielectric transition in a MT with the A lattice has features of a second order phase transition that is also indicated by the character of the curve calculated using the Monte Carlo method in Fig. 7. The numerical simulations presented here were performed for both first and second order phase transitions. In Fig. 8 is an example of a calculation performed under the assumption that the transition in a MT is a second order phase transition. In this case the sign of B in Eq. (21) becomes opposite and the term CP^5 can be neglected. Assuming that the critical temperature $T_c = 350$ K gives $A = a(T_B - T_c) = -4.58 \times 10^{33}$ N C^{-2} m^{-1}, where $T_B = 310$ K is body temperature. Under these assumptions the solution of Eqs. (21) and (24) for the polarization wave is [28]

$$P = \frac{1}{2}\left(\frac{A}{\tilde{B}}\right)^{1/2}\left\{1 - \tanh\left[\frac{1}{2\sqrt{2}}\left(\frac{A}{D}\right)^{1/2}\xi\right]\right\}. \tag{40}$$

The σ wave can be obtained by substituting Eq. (40) into Eq. (25) (setting $c_0 = c_1 = 0$). The velocity of both solutions is given by

$$v = \frac{3}{\sqrt{2}}\Gamma(AD)^{1/2}. \tag{41}$$

Since there were no reliable experimental values available for the parameters Γ and e, throughout this section they were chosen arbitrarily such that the stress variable would have realistic values. The simulation shown in Fig. 8 was performed for $\Gamma = 3.08 \times 10^{-24}$ C^2 kg s^{-1} m^{-2}, $e = -3.48 \times 10^{23}$ C^{-2} m, and $\rho_r = 0.2$. The scaling of the polarization and the stress variables was the following: $P = (A/B)^{1/2}\overline{P} = 1.16 \times \underline{10}^{-26}\overline{P}$ C m and $\sigma = 3.16 \times 10^8 \overline{\sigma}$ N m^{-2}, where $\overline{P}$ and $\overline{\sigma}$ are dimensionless scaled solutions shown in Fig 8. The initial velocity of both waves was 79.3 m s^{-1}.

The plots in Fig. 8 show that both polarization and stress wave change their shape when they collide with the impurity in the MT and after time approximately $t = 1.95 \times 10^{-8}$ s they form stationary constant solutions along the MT. The permanent stress that may be imposed in a MT in this way is a factor in its destabilization. There are other factors that may destabilize MTs: the mechanical stress that originates due to the different conformation of GDP tubulin, as was discussed in Sec. II; the presence of disassembly products in the form of ring oligomers that can laterally bind to the MT ends, causing their bending and, consequently, weakening the lateral bonds between the tubulin subunits in the MT [12]; weak points inside the MT, such as a missing molecule of tubulin or an abrupt change in the number of protofilaments [36]. Due to the stationary stress that may form by means of the mechanism described here the MT instability can reach a threshold and the MT disassembles. The larger the stationary stress the more likely the MT disassembly will be.

Initially the amplitude of the stress wave has a magnitude of about 3.45×10^5 N m^{-2}. According to the above scaling the stationary stress in Fig. 8 has an amplitude of about $\sigma = 3.16 \times 10^7 \overline{\sigma}$ N m^{-2}. This means that an interaction of a stress wave with a local defect results in higher mechanical stresses. The simulations performed have also shown that larger defects (larger density fluctuations) cause earlier formation of the stationary solutions.

We can see from the following considerations that the stresses above are realistic: The measurements reported in [9] give $E_Y = 0.5 \times 10^9$ N m^{-2} for the value of Young's modulus that characterizes longitudinal stresses in MTs. From the first model the deformation of a tubulin dimer due to the propagation of the domain wall along a MT protofilament is $\Delta R_0 / R_0 = 1.58 \times 10^{-11}/8 \times 10^{-9} = 0.002$. For these values the magnitude of the longitudinal stresses in MTs can be estimated as $\sigma = E_Y(\Delta R_0 / R_0) = 10^6$ N m^{-2}.

If both waves were moving in a medium with a constant density, the polarization wave would be a domain wall between two portions of a MT that are in the ferroelectric and paraelectric phase, respectively. Such domain walls are termed nucleation fronts. The variable polarization is an average of the dipole moments in all protofilaments at a point x along the MT. Propagation of kinks along one MT protofilament could be modeled in the same way as in Sec. III by adding a term that contains electric field to Eq. (21). Including this term would also provide a means of controlling the velocity of the kinks.

Since the MT is assumed to be at a temperature that is less than critical temperature due to the propagating nucleation front the dipoles in the MT eventually would become completely ordered in a ferroelectric phase since this phase corresponds to the minimum of the free energy (see Fig. 12). The result in Fig. 8 shows that an impurity in the MT causes the dipoles to be not completely ordered since the amplitude of the stationary solution is about one-half of the amplitude of the initial kink. Calculations have shown that the ordering of dipoles due to the collision of the waves with an impurity was also different for different Γ and e. At this place it can be pointed out that the scaling of P is such that the amplitude of the polarization kink is initially about 4 times larger than the value that was used to derive the parameters A, B, C, and D. This difference can be due to the fact that the parameters used were only estimates and also due to the model chosen.

2. First order phase transition

To perform simulations for the case of a first order phase transition the value of the coefficient B had to be artificially changed (this change, however, is still within the error of the estimate). This is because the value given in Eq. (37) yields practically identical values for T_c, T_0 and T^*, the latter be-

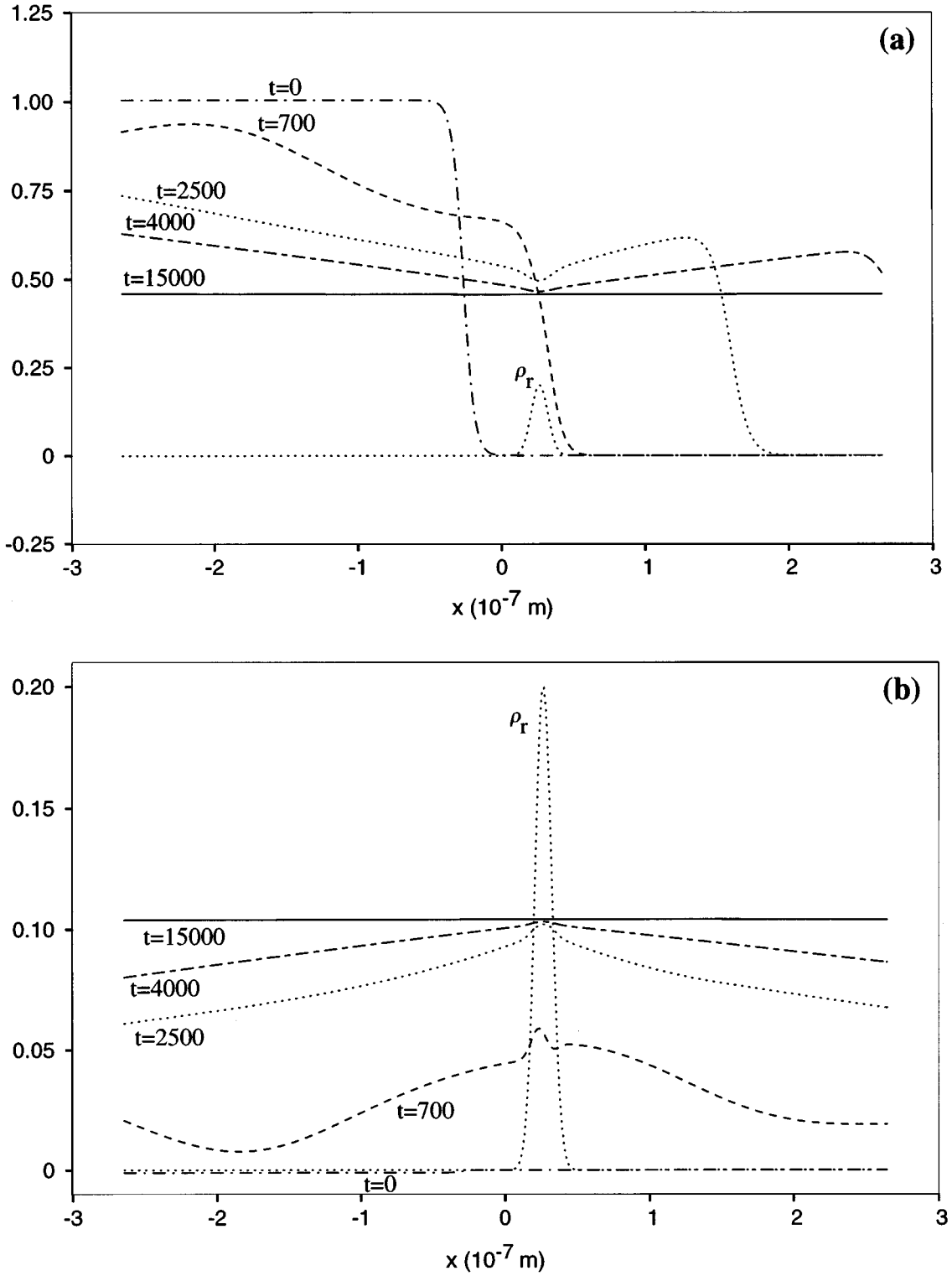

FIG. 8. Scaled solutions (40) and (25) for the values of parameters given in text: (a) polarization; (b) stress. The curves are plotted at times indicated, which are in units $(D/A)^{1/2}v_0^{-1}=1.56\times10^{-12}$ s. The amplitude of the σ kink at $t=0$ is 0.0011, which is very small on the scale of the picture.

ing the temperature at which the ferroelectric phase loses its stability (see Fig. 12). The temperatures T_0 and T^* can be calculated from the formulas [32]

$$T_0=T_c-\frac{3}{16}\frac{B^2}{aC},\quad T^*=T_c+\frac{B^2}{4aC}. \tag{42}$$

In this section the parameter B was chosen such that $B=2\sqrt{|A|C}=1.23\times10^{87}$ N$C^{-4}m^{-3}$, where A and C assume values used in the previous section. Substituting this number into Eq. (42) and keeping T_c, a, and C the same as before yields $T_0=320$ K. Since $T=T_B=310$ K, the parameter A becomes $a(T_B-T_0)=-1.14\times10^{33}$ N$C^{-2}m^{-1}$.

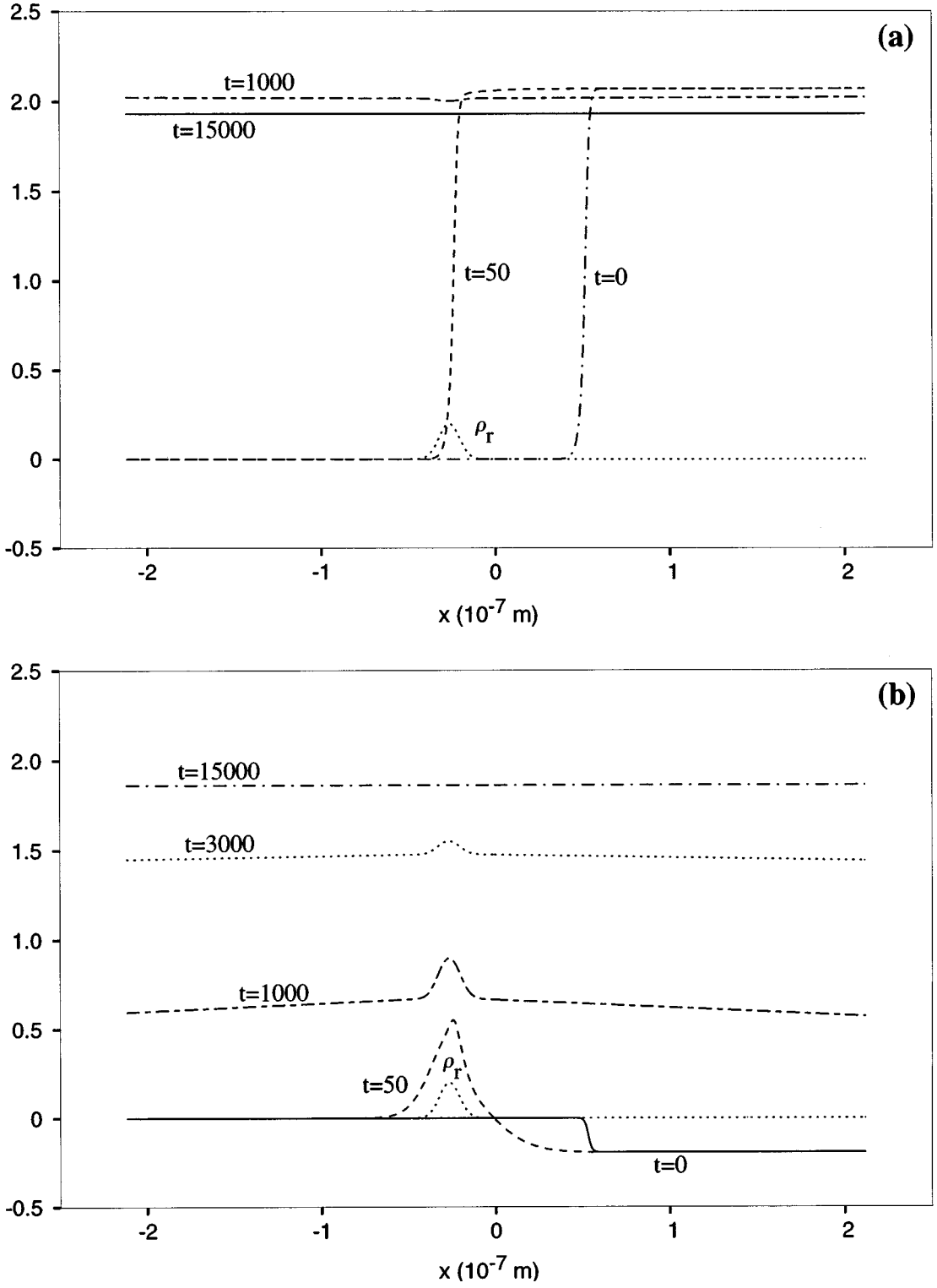

FIG. 9. Scaled solutions (28) and (25) for the given values of parameters: (a) polarization; (b) stress. The times at which the curves are plotted are in units $(D/A)^{1/2}v_0^{-1}=3.12\times10^{-12}$ s.

An example of a simulation using the modified parameters A and B is shown in Fig. 9. The calculation was performed for the values of $e=-1.25\times10^{25}$ $\mathrm{C}^{-2}\mathrm{m}$, $\Gamma=2.8\times10^{-24}$ $\mathrm{C}^2\mathrm{kg\,s}^{-1}\mathrm{m}^{-2}$ and $\rho_r=0.2$. The scaling of polarization and stress was $P=(B/4C)^{1/2}\overline{P}$ $=1.94\times10^{-27}$ $\overline{P}\mathrm{C\,m}$ and $\sigma=10^7\overline{\sigma}$ $\mathrm{N\,m}^{-2}$, where P and $\overline{\sigma}$ are dimensionless scaled solutions obtained from Eqs. (28) and (25) for $c_0=c_1=0$. The initial velocity of both waves was found by solving simultaneously algebraic equations (31) and (27). For the parameters given above the value obtained was $v=-489\ \mathrm{m\,s}^{-1}$. The minus sign means that both domain walls were moving to the left, in agreement with the minima of the free energy; i.e., the assembly of dipoles in the MT switches from the paraelectric to the ferroelectric phase.

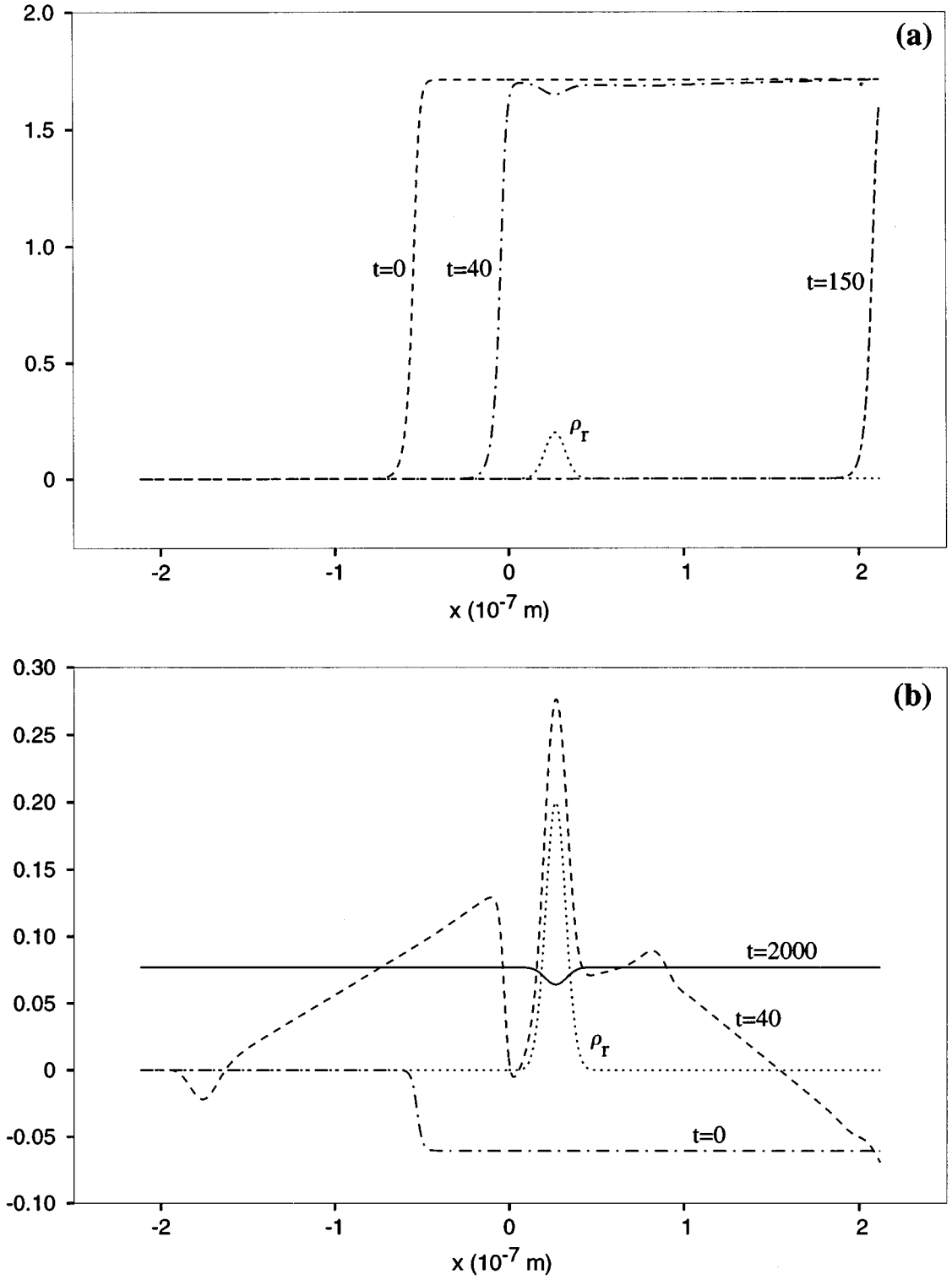

FIG. 10. Scaled solutions (28) and (25) when A is of the form (43) for $p=4.2\times10^5$ N m^{-2}: (a) polarization; (b) stress. The times at which the curves are plotted are in units $(D/A)^{1/2}v_0^{-1}=3.12\times10^{-12}$ s.

The waves could propagate in the opposite direction if A had such a value that corresponds to a temperature above critical temperature (see Fig. 12). This can be achieved by applying external pressures to the MT as will be discussed in the next section.

The results of the simulation in Fig. 9 are similar to those for the second order phase transition. Both domain walls change their shape as they approach the density fluctuation and converge to stationary solutions that have a constant amplitude along the MT after time of about $t=4.67\times10^{-8}$ s.

Adding a term that corresponds to an external electric field to Eq. (21) should have a similar effect as in the case of the second order phase transition: one of the minima of the free energy that corresponds to the ferroelectric phase would

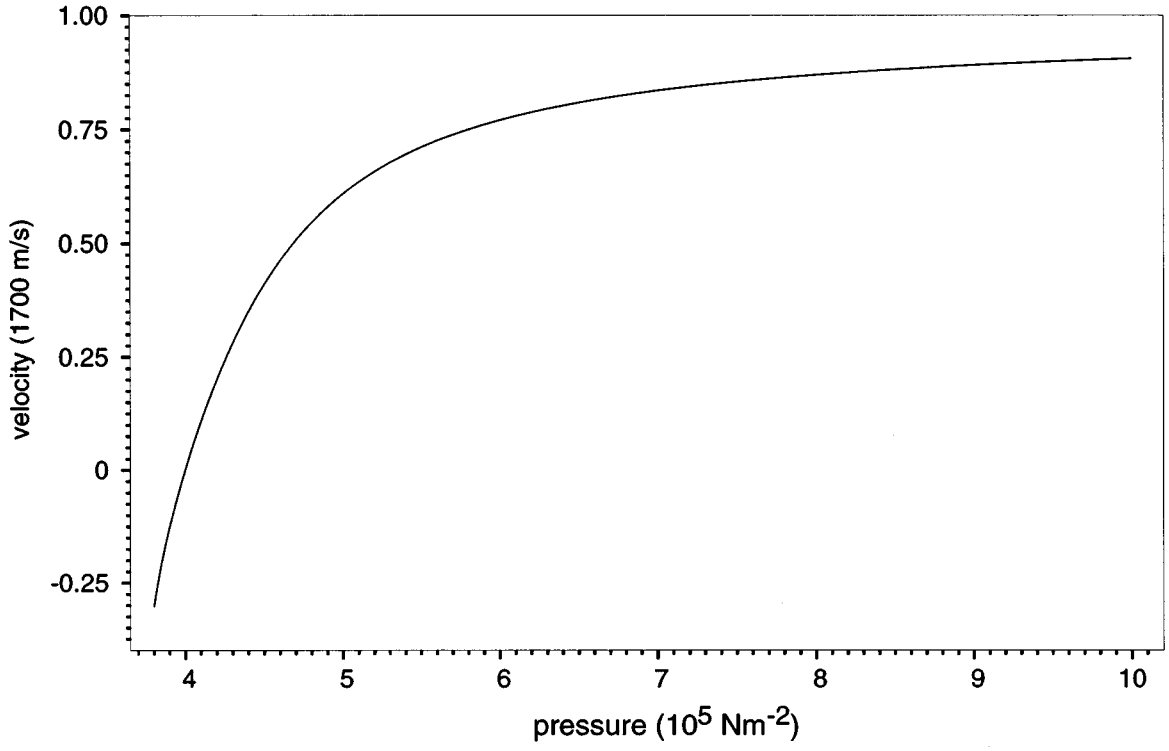

FIG. 11. A plot of the initial velocity of the polarization and stress wave as a function of pressure obtained by numerically solving Eq. (31) for the values of the parameters used to calculate the curves in Fig. 10.

be favored with respect to the other minima. Thus, the polarization kink could model a domain wall between two subchains of a MT protofilament in which the tubulin dipoles are in two different orientational states. The external electric field would also govern the velocities of the waves. To check this assumption one can construct the solution of the resulting equation of motion by means of a method described in [38].

3. Effects of pressure

Since MTs are embedded in cytosol they are subjected to hydrostatic pressures. The lowest-order interaction of the type of ferroelectric crystal that was chosen here to model the dielectric properties of MTs with hydrostatic pressure p is of the form $\Omega p P^2$, where Ω is a function of electrostrictive compliances [39]. Adding this term to the free energy (19) gives the coefficient A in the form

$$A = a(T - T_0) + 2\Omega p. \tag{43}$$

This modification could have important consequences for the propagation of kinks along MTs. The function Ω is not known for a MT. In this paper we made an assumption that it is constant and that its value is such that the term $2\Omega p$ is comparable to $|a(T-T_0)|$. Under these circumstances changing p may alter the magnitude of A significantly which affects both the sign and the magnitude of the velocity of the domain walls [Eqs. (41) and (31)].

In the case of the second order phase transition ($T_0 = T_c$) the sign of A is altered if the pressure becomes larger than $-a(T-T_c)/2\Omega$. This will inhibit the propagation of the kink waves since Eq. (26) does not have a real solution for $C=0$ and $B<0$. In the case of the first order phase transition for the values of A that correspond to temperatures $T<T_c$ the character of propagation of the solitary waves will be the same as in Fig. 9: the MT will switch from the paraelectric to the ferroelectric phase since the ferroelectric phase corresponds to the absolute minima of the free energy. When A exceeds the value that corresponds to T_c the polarization nucleation front and the stress wave will propagate in the opposite direction because the free energy has only one absolute minimum that corresponds to the paraelectric phase.

The considerations above are illustrated in Figs. 10–12. The plots of free energy in Fig. 12 correspond to Figs. 10 and 11. The parameters used to calculate the curves shown in these three figures were the same as in the previous section except for Γ, which was chosen one order of magnitude larger: $\Gamma = 2.8\times10^{-23}$ $C^2\,kg\,s^{-1}\,m^{-2}$. The parameter Ω was for convenience set to $\Omega = 1/2|a(T-T_0)|/10^5 = 5.72\times10^{27}$ $C^{-2}\,m$ and p was scaled in the units of atmospheric pressure: $p = 10^5 p$ Nm^{-2}.

The simulation shown in Fig. 10 was performed for $p = 4.2\times10^5$ $N\,m^{-2}$. This value of pressure corresponds to a temperature above T_c and therefore both polarization and stress wave move in the direction opposite to that in Fig. 9 as the MT switches from the ferroelectric to the paraelectric phase. The scaling of P and σ in this figure is the same as in Fig. 9 and gives very reasonable values for both variables. Initially both waves move with a velocity $v = 339\,m\,s^{-1}$. The time evolution of both kinks is similar to that in the simulations shown in the previous two sections: when the waves approach the defect in the MT their shape changes and after some time permanent stress forms that is constant along the MT except for a small well at the place of the density fluctuation. The MT is not polarized since it is in the paraelectric phase.

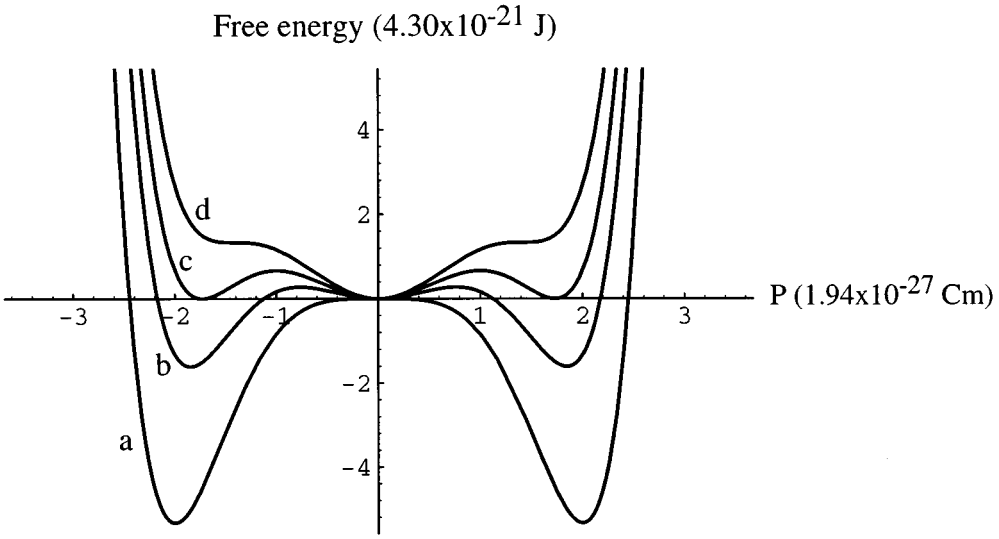

FIG. 12. Free energy $F(P,T)=1/2a(T-T_0)P^2-BP^4+CP^6$ of a ferroelectric crystal whose dipoles can be in two equivalent orientational states as a function of temperature. The crystal can undergo a dielectric first order phase transition at a critical temperature T_c. The temperature was effectively varied by replacing $a(T-T_0)$ with $a(T-T_0)+2\Omega p$ where for fixed T and T_0 different values of p were used. The plots are calculated for MT parameters given in Secs. IV A and IV A 3. (a) $T=T_0$ ($p=1\times10^5$ N m^{-2}). The paraelectric phase loses its stability. At this temperature the local minimum that corresponds to the paraelectric phase disappears and at temperatures $T<T_0$ the free energy exhibits two symmetric absolute minima that correspond to the two equivalent orientations of the dipoles in the ferroelectric phase. (b) $T_0<T<T_c$ (1×10^5 N m$^{-2}<p<4\times10^5$ N m^{-2}). The free energy has a local minimum at $P=0$ and two symmetric absolute minima that correspond to the ordered phase. (c) $T=T_c$ ($p=4\times10^5$ N m^{-2}). At the critical temperature the minima that correspond to the two dielectric phases are equivalent and the crystal undergoes a phase transition. (d) $T=T^*$ ($p=5\times10^5$ N m^{-2}). At this temperature the ferroelectric phase loses its stability: the two local minima that correspond to this phase disappear and above T^* the free energy has only one minimum at $P=0$.

Figure 11 is a plot of the initial velocity of the polarization and stress waves as a function of pressure p. This plot was obtained by numerically solving Eq. (31). As can be seen in the figure the velocity is negative for pressures less than $p=4\times10^5$ N m^{-2}. These pressures correspond to temperatures below T_c for which the free energy exhibits two symmetric absolute minima that correspond to the ferroelectric phase. This means that due to the propagating polarization wave a MT switches into the ferroelectric phase (curves *a* and *b* in Fig. 12). At $p=4\times10^5$ N m^{-2} the minima corresponding to the ferroelectric and paraelectric phases have the same depth. This is equivalent to $T=T_c$ at which the sign of the velocity changes (curve *c* in Fig. 12). For larger pressures than the above limiting value the velocity of the kinks is positive and the assembly of dipoles in a MT switches into the paraelectric phase since the free energy has only one absolute minimum at $P=0$ (curve *d* in Fig. 12). At pressures lower than $p\simeq3.8\times10^5$ N m^{-2} no kink waves exist because Eq. (31) does not have a solution for such values of p. On the other hand the solution of Eq. (31) exists for quite large pressures up to the order of magnitude 10^7 N m^{-2} (not shown in the figure). These results imply that certain pressures may inhibit the propagation of the polarization and stress domain walls on MTs. It should be noted that since depolymerization of MTs by hydrostatic pressures of about 200 atm has been reported [40] the values of pressure considered here are quite reasonable.

V. DISCUSSION

In this paper two models were used to describe quanta of energy traveling in the form of solitary waves along MTs. As has been suggested before these waves may be initiated by the free portion of the energy of the GTP hydrolysis whose role in the MT behavior is largely unknown.

The first model is represented by a partial differential equation for the elastic displacement of the tubulin dimer. The equation was set up under the assumption that a MT can undergo a second order dielectric phase transition and it includes a term that corresponds to an external electric field. Such a model can be used to describe propagation of kinklike solitary waves along a single MT protofilament. These waves may be excited by the addition of one tubulin dimer to the protofilament since the energy freed in the GTP hydrolysis that accompanies this process is comparable to the energy needed to initiate the wave. For the approximations chosen the velocity of the solitary waves depends linearly on the value of the electric field. This implies that the intrinsic electric field of a MT or the external fields from other MTs or cell membranes may control the propagation of these waves. Since the kinks may be linked to other events that involve MTs, this implies that the electric fields may govern these events. The magnitudes of the velocities for the numerical values of the parameters used are quite consistent with the experimentally measured rates of movements associated with MT motor proteins.

The motion of kinks can be slowed down by a decreasing electric field but also by a defect present in the MT whose effect can be viewed as a local potential energy barrier. At sufficiently large barriers the kink waves are stopped. The question now is what happens to the energy transported. We may speculate that it is transferred to another MT via an

attached MAP or it plays a role in the movement of a motor protein. Another suggestion is that it creates a domain wall between two portions of a MT protofilament in which the tubulin dimers are in different elastic states. This instability may be a factor in the MT disassembly.

The second model was represented by two coupled partial differential equations for the variables polarization and stress. Polarization forms a kinklike nucleation front that propagates along a MT. Hence, it may be excited by a simultaneous addition of several tubulin dimers. In the case of both first and second order phase transitions the polarization waves are domain walls between ferroelectric and paraelectric phases. When the MT is below critical temperature it switches from the paraelectric to the ferroelectric phase as the wave propagates. Above critical temperature the situation is the opposite. Collision with an impurity in the MT results in the formation of a constant stress along the whole MT. According to the simulations the amplitude of the stationary stress can be several orders of magnitude larger than the amplitude of the initial kinklike stress wave. Hence, as a result of such a collision there is a permanent stress in the MT that destabilizes it or the stress may be so large that the collision causes a destruction of the MT.

For this model we also studied the effect of external pressure on a MT. According to the results the external pressure may effectively enlarge the temperature of the MT so that it exceeds the critical temperature. This would change the dielectric phase of the MT. The pressure also affects the velocity of the kinks and for certain pressures the kinks do not propagate at all. Thus, the hydrostatic pressure to which a MT is subjected in the cellular environment may act in some circumstances as a kink inhibitor.

It can be noticed that the values of the velocities of the waves obtained in the second model are several orders of magnitude larger than the velocities obtained in the first model. For $\epsilon_r = 70$ and the charge of the dipole equal to a few electronic charges the velocities of the waves described by the second model were about $10^2\ \mathrm{m\,s^{-1}}$ and for the first model they would be $10^{-2}-10^{-5}\ \mathrm{m\,s^{-1}}$ (note that the velocity of sound is $1700\ \mathrm{ms^{-1}}$). However, the second model was analyzed neglecting the presence of an external electric field, which was incorporated into the equation of motion that represents the first model. The electric field acted as a mean of control of the magnitudes of the velocities of the kinks. Thus, the two models can be made more comparable by incorporating the term that corresponds to the external electric field into the equations of motion of the second model.

[1] S. Rasmussen, H. Karampurwala, R. Vaidyanath, K. S. Jensen,and S. Hameroff, Physica D **42**, 428 (1990).

[2] S. R. Martin, M. J. Schilstra, and P. M. Bayley, Biophysical J. **65**, 578 (1993).

[3] B. Alberts, D. Bray, J. Lewis, M. Raff, K. Roberts, and J. D. Watson, *Molecular Biology of the Cell*, 3rd ed. (Garland Publishing, New York, 1994).

[4] *Microtubules*, edited by J. S. Hyams and C. W. Lloyd (Wiley-Liss, New York, 1994).

[5] T. J. Mitchison and M. W. Kirschner, Nature **312**, 232 (1984); Nature **312**, 237 (1984).

[6] E. Mandelkow and E.-M. Mandelkow, Current Opinion Cell Biol. **2**, 3 (1990).

[7] M. Kirschner and T. Mitchison, Cell **45**, 329 (1986).

[8] K. Kirchner and E.-M. Mandelkow, EMBO J. **9**, 2397 (1985).

[9] B. Mickey and J. Howard, J. Cell Biol. **139**, 909 (1995).

[10] M. Caplow, R. L. Ruhlen, and J. Shanks, J. Cell Biol. **127**, 779 (1994).

[11] E.-M. Mandelkow, E. Mandelkow, and R. A. Milligan, J. Cell Biol. **114**, 977 (1991).

[12] A. Marx and E. Mandelkow, European Biophys. J. **22**, 405 (1994).

[13] Kuo-Chen Chou, Chun-Ting Zhang, and G. M. Maggiora, Biopolymers **34**, 143 (1994).

[14] M. V. Satarić, R. B. Žakula, and J. A. Tuszyński, Phys. Rev. E **48**, 589 (1993).

[15] M. V. Satarić, Dj. Koruga, Z. Ivić, and R. Žakula, J. Mol. Electron. **6**, 63 (1990).

[16] M. V. Satarić, R. Žakula, and J. A. Tuszyński, Nanobiology **1**, 445 (1992).

[17] A. Gordon, Phys. Lett. A **154**, 79 (1991).

[18] H. Athenstaedt, Ann. N.Y. Acad. Sci. **238**, 68 (1974).

[19] H. Fröhlich, Proc. Natl. Acad. Sci. (U.S.A.) **72**, 4211 (1975).

[20] S. Hameroff, *Ultimate Computing* (North-Holland, Amsterdam, 1987).

[21] J. A. Tuszyński, B. Trpišová, D. Sept, M. V. Satarić, and S. R. Hameroff, in *Proceedings of the Conference Toward a Science of Consciousness*, edited by S. R. Hameroff, A. W. Kaszniak, and A. C. Scott (MIT Press, Cambridge, 1996), pp. 407–418.

[22] J. M. Yeomans, *Statistical Mechanics of Phase Transitions* (Clarendon Press, Oxford, 1992)

[23] Y. M. Sirenko, M. A. Stroscio, and K. W. Kim, Phys. Rev. E **53**, 1003 (1996).

[24] M. B. Hakim, S. M. Lindsay, and J. Powell, Biopolymers **23**, 1185 (1984).

[25] J. F. Currie, A. Blumen, M. A. Collins, and J. Ross, Phys. Rev. B **19**, 3645 (1979).

[26] P. M. Vassilev, R. T. Dronzine, M. P. Vassileva, and G. A. Georgiev, Bioscience Rep. **2**, 1025 (1982).

[27] H. Bolterauer, J. A. Tuszyński, and M. V. Satarić, Phys. Rev. A **44**, 1366 (1991).

[28] J. M. Dixon, J. A. Tuszyński, and M. Otwinowski, Phys. Rev. A **44**, 3484 (1991).

[29] J. A. Tuszyński, B. Trpišová, D. Sept, M. V. Satarić, and S. Hameroff, in *Proceedings of the Conference Nonlinear Excitations in Biomolecules*, Les Houches School, 1994, edited by M. Peyrard (Springer, Berlin, 1995), pp. 387–404.

[30] D. K. Fygenson, E. Braun, and A. Libchaber, Phys. Rev. E **50**, 1579 (1994).

[31] A. Gordon, Physica B **138**, 239 (1986).

[32] A. Gordon and S. Dorfman, Phys. Rev. B **50**, 132 (1994).

[33] L. D. Landau and E. M. Lifshitz, *Electrodynamics of Continu-*

ous Media (Pergamon Press, Oxford, 1960).
[34] L. D. Landau and I. M. Khalatnikov, Dokl. Akad. Nauk SSSR **96**, 469 (1954) [English translation in *Collected Papers of Landau*, edited by D. ter Haar (Pergamon Press, Gordon and Breach, London, 1965)].
[35] J. A. Tuszyński and D. Sept, J. Phys. Condens. Matter **6**, 3583 (1994).
[36] E. Mandelkow and E.-M. Mandelkow, Current Opinion Struct. Biol. **4**, 171 (1994).
[37] J. A. Tuszyński and W. Wierzbicki, Am. J. Phys. **59**, 555 (1991).
[38] M. Otwinowski, R. Paul, and W. G. Laidlaw, Phys. Lett. A **128**, 483 (1988).
[39] G. A. Samara and P. S. Peercy, *Solid State Physics, Advances in Research and Applications*, Vol. 36, edited by H. Ehrenreich, F. Seitz, and D. Turnbull (Academic Press, New York, 1981), pp. 2–118.
[40] Shinya Inoue, J. Struct. Biol. (to be published).